A Model-Driven Bayesian Method for Polyp Detection and False Positive Suppression in CT Colonography Computer-Aided Detection

Xujiong Ye and Greg Slabaugh

R&D Department, Medicsight PLC, London, UK

ABSTRACT

This chapter presents an automated method to identify colonic polyps and suppress false positives for Computer-Aided Detection (CAD) in CT Colonography (CTC). The method formulates the problem of polyp detection as a probability calculation through a unified Bayesian statistical approach. The polyp likelihood is modeled with a combination of shape, intensity and location features, while also taking into account the spatial prior probability encoded by a Markov Random Field. A second principal curvature PDE provides a shape model; and partial volume effect is incorporated in the intensity model. When evaluated on a large multi-center dataset of colonic CT scans, the CAD detection performance as well as the volume overlap ratio demonstrate the potential of the proposed method. The method results in an average 24% reduction of false positives with no impact on sensitivity. The method is also applicable to generation of initial candidates for CTC CAD with high detection sensitivity and relatively lower false positives, compared to other non-Bayesian methods.

Keyword: Bayesian statistics; Computer-Aided Detection; Colonic polyp detection; False positive reduction; Markov random field; Principal curvature; PDEs.

1 INTRODUCTION

Colorectal cancer (CRC) is the second leading cause of cancer related death in western countries. Early detection and removal of polyps has been associated with reduction in the incidence of colorectal cancer (Winawer *et al*., 2003). As a new minimally-invasive screening technique, computed tomography (CT) colonoscopy (CTC), also more popularly known as virtual colonoscopy (VC), uses CT imaging and dedicated interactive three-dimensional (3D) and two-dimensional (2D) imaging software to evaluate the colon. CTC has shown several advantages over the traditional optical colonoscopy (OC) for screening (Pickhardt *et al*., 2003). Clinical studies suggest CTC can provide similar detection performance as colonoscopy but has a reduced risk of complication (Kim *et al*., 2007). The CT scan is performed in supine and prone positions during a breath-hold acquisition. No sedation or analgesics are required.

Although CTC has been demonstrated to be an effective alternative colorectal screening approach (Johnson *et al*., 2008) , the manual interpretation of the CT data sets is very time-consuming due to the large quantity of data generated (typically 800-2000 images per patient) and some key factors (such as reader experience and specific skills) can affect the quality of CTC interpretation. Computer-aided detection (CAD) for CTC has been developed for the automated detection of polyps in order to overcome the difficulties of manual CTC interpretation. CAD offers the radiologist a second opinion, and has been shown to reduce the variability of the procedure. The clinical impact of CAD is being investigated. CTC CAD has been suggested as an effective second reader and may enhance the efficacy of CTC examinations through increased sensitivity of CTC examinations (Lawrence *et al*., 2010).

1.1 Background

As a promising technology for CTC screening, colon CAD has received considerable research interest. Early effort of CTC CAD started with the work of Vining *et al.* (1999), who identified polyps based on colonic wall thickness. Since then, several polyp detection methods were developed. To date, typical

approaches to CTC CAD can be classified as *shape-based*. Most sessile and pedunculated polyps protrude from the colon lumen and can be identified by their shape, which is part or totally spherical. Shape-based methods often rely on shape features derived from either first order differential geometric quantities, such as gradient concentration (GC) (Yoshida *et al*., 2001), surface normal overlap (SNO) (Paik *et al*., 2004), etc; or from second order quantities computed using Hessian matrices (Koenderink *et al*., 1992; Yoshida *et al*., 2001; Summers *et al*., 2005), such as principal, mean, or Gaussian curvatures, etc. Yoshida and Nappi (2001; 2002) compute shape index and curvedness from principal curvatures to find initial candidates, which are then clustered and classified using quadratic discriminant analysis. They also add gradient concentration (GC) and directional gradient concentration (DGC) features in the CAD in order to improve performance. GC and DGC calculate the confluence of gradient vectors toward a common point, while Paik *et al*. (2004) apply surface normal overlap method which is similar to the gradient orientation calculation but with statistic shape formulation. The work of Summers *et al.* (2005) utilizes mean curvature computed at voxels on the mucosal surface, which are then clustered and classified using quadratic discriminant analysis, whereas Kim *et al.* (2007) rely on eigenvalues of the Hessian matrix. Instead of computing curvature information on the voxel grid, Sundaram *et al.* (2008) apply a geometry processing approach directly on a mesh-based representation of the colon. Van Ravesteijn *et al*. (2010) use the second principal curvature in a differential equation that is solved explicitly on a mesh or implicitly on the image grid to identify polyp candidates. Jerebko *et al.* (2006) extended the work of Bogoni *et al.* (2005) by analyzing the symmetry of curvature patterns of raised objects in the colonic lumen.

Shape based methods have made steady progress in achieving high detection sensitivity and relatively low false positive regions (FPs). This is because the shape features take advantage of the fact that polyps tend to have rounded shapes or contain at least local spherical elements; while colonic folds are elongated shapes. However, in practice, polyps are often abnormal growths that exhibit varying morphology, and shape-based methods may fail to detect polyps with sufficient reliability. Therefore, further improvement

is needed to provide a more accurate and reliable detection of polyps. In addition to shape-based features, other features such as those based on appearance or location can also be used to improve detection performance. Appearance based features commonly employed in CTC CAD algorithms include image intensity, statistical measures of intensity histograms, and/or texture features. These features take advantage of the fact that polyps typically exhibit a slightly elevated intensity and inhomogeneous texture relative to surrounding mucosal tissue. In this chapter, we use the image intensity as an appearance feature. Distance features can be used to model the likelihood of polyps appearing in different locations in the human anatomy.

The goal of this chapter is to combine shape features with appearance and location features to produce a robust detector in a unified Bayesian framework. The advantages of a Bayesian technique are as follows. First, a Bayesian statistical technique is ideally suited to modeling the large uncertainty inherent to detection problems in medical imaging. Second, there often is useful medical knowledge (such as lesion density, size, shape, location, etc.) that can be utilized to constrain the solution of detection problems. This prior medical knowledge can be easily encoded into a Bayesian model through the prior probabilities. Finally, a Bayesian technique provides a unified framework to incorporate various features F into one statistical model.

A complete CTC CAD system consists of the following four steps: colon segmentation; initial candidate generation; feature calculation and classification / candidate filtering. Bayesian models have appeared in various CAD approaches (Zrimec *et al.*, 2007; Raykar *et al.*, 2008). However, they are typically incorporated at the last stage of CAD, i.e., the classifier stage, and applied to candidate regions generated using other detection methods mentioned earlier. For each candidate region, global features are calculated within the region and then formulated into Bayesian classifier to determine the probability of the region being a polyp region. These methods rely on proper region segmentation for accurate feature calculation. In contrast to such work, Mendonca *et al*. (2007) form a probability distribution function for each voxel in the CT image, initially for pulmonary nodule detection, and then extend the work to colonic structures (2008). Simple analytical models are sampled using an appropriate sampling procedure and the

sample points are then mapped on the model to curvature values using either classical differential geometry or the geometry of Gaussian random fields. The method assigns each voxel with a probability value being polyp. This voxel labeling method bypasses the segmentation step by incorporating information from neighboring voxels in a predefined way and calculating voxel probability only at a local feature level.

1.2 Our contribution

In this chapter, we present a unified Bayesian framework incorporating shape, appearance, and location features for estimating the probability that a voxel is contained within a polyp. Compared to the work in Mendonca *et al.* (2007, 2008), there are two main differences. First, Mendonca *et al*. apply simplified geometric models (ellipsoidal polyps, spherical colon wall, etc.) for modeling shape features. Such models have limited capability to represent the complexity of actual polyps found in human anatomy. In contrast, our approach relies on more expressive shape model that has been shown to model the variation in polyp shapes seen in practice. Second, Mendonca *et al.'s* method precludes a specific training step and only medical knowledge is used in modelling the prior probability. However, our framework includes prior medical knowledge through explicit learning based on labeled examples, as well as modeling local interactions between voxels through a Markov Random Field. Essentially, our method endows each voxel with a "polypness" value, indicating its probability of being located within a polyp. To our knowledge, this is the first time such a learning-based Bayesian approach for modeling the likelihood of polyp voxels has been proposed in a CTC CAD system. The method is utilized in one of two ways:

1) Initial detection of potential polyp candidates, i.e., candidate generation.
2) Removal of unlikely polyp candidates, i.e., candidate filtering.

Compared to our previous work (Ye et al., 2010), there are two main contributions. First, in our earlier work, a uniform prior is used in the Bayesian probability calculation; while in this chapter, we have modeled the Bayesian prior probability by considering local interactions between voxels through a

Markov Random Field (MRF). Our experimental results on candidate filtering show that by considering MRF in the prior probability, the proposed method can achieve an average 24% reduction of FPs with no impact on sensitivity, which improves the FP reduction by an average of 8%, compared to that using a uniform prior. Secondly, in this chapter, we have also investigated the method on the candidate generation of the CAD system for both the detection performance and the volume overlap ratio. Two intensity models are used based on different applications of the candidate generation and candidate filtering. The experimental results on a large multi-center clinical dataset of colonic CT scans demonstrate the excellent detection performance with high sensitivity and fewer FP regions, even for polyps on colonic folds.

2. METHOD

We are given a set of voxels $X=\{x_i,\ i=1,\ldots,N\}$ in a 3D image, a set of features $F=\{F_j,\ j=1,\ldots,M\}$ associated with each voxel x_i, and a set of labels $\Lambda=\{l_1..l_K\}$. Here, we use K=2, where, l_1 is a non-polyp label; while l_2 is a polyp label. This section focuses on assigning one of the labels to an individual image voxel based on a probability calculation using a combination of features through a unified Bayesian framework. Three features are considered: the intensity I, shape S and location L; namely, $F_1=I$, $F_2=S$, $F_3=L$. Although we focus on these three features, the framework is extensible to other features as well. In general, the features for the Bayesian probability can be any 2D or 3D feature for lesion detection.

Let $R=\{R_1,\ldots,R_N\}$ be a family of random variables in which R_i takes a value $r_i \in \Lambda$, i.e., r_i is the label for voxel x_i. The symbol $P(\mathrm{X}|\mathrm{F})$ denotes the conditional probability of the random variable R_i that takes value of $r_i= l_2$ at x_i in the probability space, namely $P(\mathrm{X}|\mathrm{F})= P(r_i=l_2|\mathrm{F})$. Based on Bayes' law, we have:

$$P(X|F)=\frac{P(F|X)\cdot P(X)}{P(F)} \tag{1}$$

where, the posterior, likelihood, and prior terms are $P(\mathrm{X}|\mathrm{F})$, $P(\mathrm{F}|\mathrm{X})$ and $P(\mathrm{X})$, respectively, and $P(\mathrm{F})$ is a normalization term.

Assuming each feature being conditionally independent, Equation 1 can be written as:

$$P(X|F) = \frac{P(F_1|X) \cdot P(F_2|X) \cdot P(F_3|X) \cdot P(X)}{P(F_1) \cdot P(F_2) \cdot P(F_3)} \quad (2)$$

Given $F_1 = I$, $F_2 = S$, $F_3 = L$, therefore,

$$P(X|I,S,L) \propto P(I|X) \cdot P(S|X) \cdot P(L|X) \cdot P(X)$$

The overarching goal of this work is to use Equation 2 to model the probability of a polyp label existing at each voxel in the CT colon volume. Essentially, this endows each voxel with a "polypness" value that describes the likelihood the voxel represents a polyp voxel. A block diagram of the proposed method is illustrated in Fig. 1. Below, each stage is described in detail.

Figure1 Block diagram of the proposed Bayesian method

2.1 Modeling the likelihood term

In the Bayesian framework, the likelihood term indicates the joint density distribution of all features for class l_2. In this section, each feature model is described in detail. It is noted that, to accurately calculate each feature, during the pre-processing step, a Gaussian filter is applied on the whole 3D volume to remove noise.

2.1.1 Shape model

The second principal curvature (K2) partial differential equation (PDE, or *flow*) for polyp detection was recently introduced by van Wijk *et al*. (2010). The aim of this section is to model the K2 PDE's feature distribution and combine it into the joint statistical likelihood term of the Bayesian framework.

The vast majority of polyps are raised objects protruding from the colon surface, which means their first and second principal curvatures have positive values. In contrast, colonic folds are elongated structures, bent only in one direction, and correspondingly exhibit a positive first principal curvature and a close to zero second principal curvature. Therefore, to detect polyps, a flow based on the second principal curvature can be designed that affects only points with a positive second principal curvature in such a way that the second principal curvature decreases. Repeated application of the PDE on an image will gradually deform the image, reducing, and then removing surface protrusions.

A PDE flow to remove protruding objects can be defined as:

$$\frac{\partial I}{\partial t} = -g\left(k_1(x_i), k_2(x_i)\right) \cdot \left|\nabla I\right| \tag{3}$$

where $\left|\nabla I\right|$ is the gradient magnitude of the 3D image, and $g(\cdot)$ is a curvature dependent function characterizing the flow, $k_1(x_i)$ and $k_2(x_i)$ are the first and second principal curvatures at voxel x_i of the 3D image, computed directly from image intensity through Gaussian ($K(x_i)$) and mean ($H(x_i)$) curvatures defined as (Monga & Benayoun, 1995; Thirion & Gourdon, 1992):

$$k_1(x_i) = H(x_i) + \sqrt{H^2(x_i) - K(x_i)}, \qquad k_2(x_i) = H(x_i) - \sqrt{H^2(x_i) - K(x_i)} \tag{4}$$

The calculation of the Gaussian and mean curvatures are based on the first and second fundamental forms of differential geometry, which can be computed as:

$$K(x_i) = \frac{LN - M^2}{EG - F^2}, \qquad H(x_i) = \frac{EN - 2FM + GL}{2(EG - F^2)} \tag{5}$$

where:

$$E = 1 + \frac{f_x^2}{f_z^2}, \qquad F = \frac{f_x f_y}{f_z^2}, \qquad G = 1 + \frac{f_y^2}{f_z^2}$$

$$L = \frac{2 f_x f_z f_{xz} - f_x^2 f_{zz} - f_z^2 f_{xx}}{R}, \quad M = \frac{f_x f_z f_{yz} + f_y f_z f_{xz} - f_x f_y f_{zz} - f_z^2 f_{xy}}{R}, \quad N = \frac{2 f_y f_z f_{yz} - f_y^2 f_{zz} - f_z^2 f_{yy}}{R}$$

$$R = f_z^2 \sqrt{|f|}, \qquad |f| = \sum_{i=x,y,z} f_i^2 \tag{6}$$

here, f_x, f_y, f_z, f_{xy}, f_{yz}, f_{xz}, f_{xx}, f_{yy}, f_{zz} are the first and second–order partial derivatives of the image with respect to *x*, *y*, *z*, respectively.

In this study, the aim is to have a small flow on colonic folds; while producing a large response on protruding objects (such as polyps). Therefore, the flow to remove protruding objects can be defined as:

$$\frac{\partial I}{\partial t} = \begin{cases} -k_2(x_i) \cdot |\nabla I| & (k_2(x_i) > 0) \\ 0 & (k_2(x_i) < 0) \end{cases} \tag{7}$$

Based on Equation 7, the image intensities exhibit small (if any) change for colonic folds, and large change for protruding objects (such as polyps). During each iteration, only at locations of protruding objects where the second principal curvature is positive, the image intensity is reduced by an amount proportional to the local second principal curvature k_2. After the PDE reaches steady state, the difference image *D* between the deformed and the original 3D images indicates the amount of protrusion. By design, it discriminates between polyps and folds and is robust to different polyp morphologies and sizes.

A truncated Gaussian function is used to model the polyp likelihood as a function of the intensity difference $F_1^{k2} = D$. The truncated Gaussian function allows a larger range of voxels with high K2 flow intensity differences to have high probability of being a polyp,

$$P(F_1^{k2} | X) = \exp\left(-\frac{(F_1^{k2} - \mu_{k2})^2}{\delta_{k2}^2} \right), \textit{when } F_1^{k2} > \mu_{k2}, \; P(F_1^{k2} | X) = 1 \tag{8}$$

where μ_{k2} and δ_{k2} are the mean and standard deviation (*std*), respectively, determined through a training dataset.

Alternatively, as mentioned earlier, any other second order shape feature, such as shape index used in (Yoshida *et al*., 2001), can be used to model the shape likelihood. The volumetric shape index at voxel x_i can be defined as (Monga & Benayoun, 1995; Thirion & Gourdon, 1992):

$$F_1^{SI}(x_i) = \frac{1}{2} - \frac{1}{\pi} \arctan \frac{k_1(x_i) + k_2(x_i)}{k_1(x_i) - k_2(x_i)} \tag{9}$$

The shape index has been widely used in lesion detection. It provides a local shape feature at each voxel that directly characterizes the topological shape of an iso-surface in the vicinity of each voxel without explicitly calculating the iso-surface. Similar to the K2 shape feature of Equation 8, the likelihood of shape index feature can also be modeled using a Gaussian function. In Section III of this chapter, the CAD performance of using volumetric shape index likelihood is compared to that of the K2 shape feature.

2.1.2 Intensity model

It is well known that CT images exhibit partial volume effect (PVE) due to the limitations in scanning resolution. For tissues like polyps near air, the boundary of the polyp may appear darker than that of its central region as a result of the PVE. For simplicity, assume that a polyp is in hemispherical in shape and contains two parts: a core part (r_c) with mean intensity μ_{Ic} and a PVE part (Δr) with the mean intensity μ_{Ip}. Fig. 2 shows the schematic diagram. Two intensity models can be used based on different applications.

Fig.2 A schematic diagram of colonic polyp

As mentioned in Section 1.2, the Bayesian approach can be used either in the candidate generation or candidate filtering steps of the CAD system. For candidate generation, the parametric form of the polyp intensity model can be given by a two-mixture Gaussian function:

$$P(F_2|X) = c_1 \exp\left(-\frac{(I-\mu_{Ic})^2}{\delta_{Ic}^2}\right) + c_2 \exp\left(-\frac{(I-\mu_{Ip})^2}{\delta_{Ip}^2}\right) \tag{10}$$

where $\sum_{i=1,2} c_i = 1$, δ_{Ip} and δ_{Ic} are the *std* for each Gaussian function. The parameters can be estimated by application of the expectation-maximization (EM) algorithm (Webb, 1999) using a training dataset.

In the candidate filtering (FP reduction) case, the candidate region's size is available and can be incorporated into the model to address the PVE. The polyp intensity model varies for each polyp region and can be given by a Gaussian function:

$$P(F_2|X) = \exp\left(-\frac{(F_2-\mu_I(r))^2}{\delta_I^2}\right) = \exp\left(-\frac{(I-\mu_I(r))^2}{\delta_I^2}\right) \tag{11}$$

where $\mu_I(r)$ is the mean intensity and can be defined as a function of potential polyp size (e.g. radius r). Given the whole polyp radius as $r = r_c + \Delta r$, the mean intensity of a polyp is adaptively determined as:

$$\mu_I(r) = f \cdot \mu_{Ic} + (1-f) \cdot \mu_{Ip} \tag{12}$$

where f is the fraction of the core part's volume compared to the whole polyp's volume, namely,

$$f = r_c^3 / r^3 = (r-\Delta r)^3 / r^3 \tag{13}$$

When a polyp is very small, there might not be a core part, namely $r_c = 0$ and $f = 0$, therefore, $r = \Delta r$; that is to say, the polyp only contains a PVE part, so the mean intensity μ_I depends on the mean intensity of PVE μ_{Ip}. In contrast, when a polyp is very big, e.g. $r \to \infty$, we have $f = 1$, so the mean intensity μ_I

depends on the mean intensity of core part μ_{Ic}. Fig. 3 shows an example of how the mean intensity of the polyp varies with radius size, where, $\Delta r = 0.25$, $\mu_{Ic} = 150HU$, $\mu_{Ip} = -175HU$, obtained through the training dataset mentioned in Section 2.3.

Fig.3 An example of how mean intensity of the polyp varying with the radius size based on Equation 12.

2.1.3 Distance model

Distance features, based on prior medical knowledge, can also be combined into Bayesian framework for polyp detection. Two types distance features are considered in this work. A first distance feature is the distance to the colon mucosal surface (F_3^{CS}). This is based on the observation that polyps are typically located on or near the colon. Voxels closer to the colon surface have a higher probability of being labeled as polyp voxels, compared to voxels farther away. Another distance feature is the distance to the rectum (F_3^{CL}). This feature is based on prior medical knowledge that polyps are typically more prevalent in lower extremities of the colon (i.e., in the rectum and sigmoid) rather than farther up the colon anatomy (towards the caecum).

In this chapter, the distance to the colon mucosal feature (CS) is considered. To calculate CS feature, the 3D boundary distance transform (Gonzalez & Woods, 2002) is applied to the segmented colon. For each voxel in 3D image, the distance to the colon surface (F_3^{CS}) can be obtained based on the distance transform map and the maximum distance d_{max} within the segmented colon to the boundary can be calculated. A linear function $P(F_3|X)$ is then used to model the polyp distance likelihood as follows:

$$P(F_3|X)=\begin{cases}1 & , \quad F_3^{CS} < f_\mu \cdot d_{\max} \\ 1-\dfrac{F_3^{cs}-f_\mu \cdot d_{\max}}{(f_{\max}-f_\mu)\cdot d_{\max}} & , \quad F_3^{CS} \geq f_\mu \cdot \mathrm{d}_{\max}\end{cases} \tag{14}$$

where both f_μ and $f_{\max}$ are the positive factors controlling the size of voxels being considered in the polyp likelihood calculation, which can be set to be 0.3 and 0.5, respectively. Based on Equation 14, the distance probability map is adaptive to the size (or maximum distance) of the segmented colon.

2.2 Modeling the prior term

Due to the spatial dependence in the human body, voxels with the different intensity may have the same structural properties. In this chapter, this spatial property can be encoded into the Bayesian prior probability. The spatial prior *P*(X) in Equation 1 can then be constrained by spatial information imposed by a Markov Random Field and Gibbs Random Field (MRF-GRF).

In an MRF, only neighboring voxels have direct interactions with each other and they tend to have the same class label. According to the Hammersley-Clifford theorem, the spatial prior probability can be derived using MRF-GRF equivalence as follows (Li, 1995):

$$p(x_i)=p(r_i=l_2)\approx p\left(x_i\middle|x_{N(i)}\right)=\frac{\exp\left[-\sum_c v_c(r_i=l_2)\right]}{\sum_{r_i\in\Lambda}\exp\left[-\sum_c v_c(r_i)\right]} \tag{15}$$

where $N(i)$ is the neighborhood of voxel *i*. $v_c(x_i)$ is a potential function associated with the clique *c* defined as: $v_c(r_i=l_2)=-\beta\cdot p(x_i|F)$ and $v_c(r_i=l_1)=-\beta\cdot(1-p(x_i|F))$, β is a positive factor controlling the size of clustering. In this study, a second-order neighborhood system and pairwise interaction clique between neighbors are considered.

It can be seen that the prior probability of voxel *i* being a polyp voxel depends on its neighborhood probability. If its neighboring voxels are labeled as polyp voxels, a voxel has higher probability to be

labeled as polyp; similarly, if its neighboring voxels are non-polyp, the voxel has lower probability to be labeled as polyp.

2.3 Training

As discussed in the above section, each feature distribution can be modeled through Equations 8-14. The parameters related to each model are estimated using a training step as discussed below.

In the training set, there are 68 CTC annotated volumes from six different hospitals. Each polyp boundary was manually delineated by a qualified radiologist, and the dataset consists of 70 polyps in total. The training set is used to optimize model parameters. In this study, each feature likelihood term in Equation 1 is associated with one rule for polyp detection. The parameters for each model that provide a good cut-off in a ROC curve are chosen.

As an example of estimating the optimal model parameters (μ_{Ic} and μ_{Ip}) for intensity likelihood (Equation 10-12), the intensity distribution for all the ground truth polyps in the training set is firstly calculated, and the EM algorithm is then applied to estimate model parameters, where, in Equation 10, we have $\mu_{Ic} = 150HU$, $\mu_{Ip} = -175HU$, $\delta_{Ip} = \delta_{Ic} = 50$ and c_1, c_2 are 0.82 and 0.18, respectively.

Similar to the intensity model, the optimal parameters for shape models (Equation 8) from the EM algorithm for the training set can be estimated as $\mu_{k2} = 235.0$ and $\delta_{k2} = 50.0$.

3. EXPERIMENTAL RESULTS AND DISCUSSION

The trained Bayesian model has been evaluated on an independent CTC dataset. As mentioned in Section 1.2, the proposed method can be used in CAD in one of two ways: candidate generation or candidate filtering. We vary the intensity model, as described in Section 2.2, Equations 10-11, depending on the application. Experiments have been conducted to demonstrate the effectiveness of the proposed algorithm applied to both steps.

3.1 Candidate generation

We applied the proposed method to the candidate generation step of CAD, which identifies initial potential polyps from the 3D image. The process is as follows:

1) Extract colon mask based on fuzzy thresholding (Slabaugh *et al*., 2010) .
2) Calculate the conditional probability map. For each voxel x_i in 3D image,
    a. Calculate shape likelihood, intensity likelihood and distance likelihood based on Equations 8, 10 and 14, with the model parameters estimated from the training set mentioned in Section 2.3. Note that the distance probability map calculated from Equation 14 provides a mask for both shape and intensity probability calculation. Voxels far away from the colon surface having very low or zero distance probability will have less probability to be labeled as polyp. Therefore, to speed up the computation time, both the shape and intensity probabilities can be only calculated within a band around the colon mask.
    b. Calculate the prior spatial probability based on Equation 15, where β is chosen to be 1.0.
    c. Calculate the conditional probability of being labeled as polyp (l_2) for each voxel x_i based on Equation 1.
3) Hysteresis thresholding (Yoshida *et al.*, 2001) is applied to the conditional probability map to obtain binary image.
4) 3D labelling then groups 3D connected regions.
5) For each 3D connected region, if the size of the region is larger than a pre-defined threshold, then keep the region as one of the initial potential polyp candidates, otherwise, remove the region from the list of candidates.

Fig. 4 shows examples of detection of two polyps (with one polyp attached to the colon wall, while the other polyp is attached to a colonic fold). For the shape model in Equation 2, the second principal curvature flow (K2) (Equation 8) is compared with shape index (SI) feature (Equation 9). Note that the distance feature is not included in this experiment, since in this experiment, the Bayesian method is applied to sub-images to compare the polyp detection performance using K2 and SI as the shape model. It can be seen that, both the intensity likelihood map (Equation 10, Fig.4b) and the shape likelihood map (Equation 8 and 9) are highlighting the polyps. However, compared to using the SI as the shape model (Fig.4c), the proposed K2 shape feature (Fig. 4e) shows superior performance with very few false regions in the entire sub-image. Fig. 4(f) is the final polyp probability map from the joint intensity and K2 shape feature likelihoods (Equation 2). It can be seen that, by using the proposed Bayesian method with K2 shape feature, both polyps can be detected and properly segmented from the surrounding tissues.

A quantitative evaluation has also been conducted. An independent dataset of 66 CT colon scans with 93 polyps is used in this experiment. Both the detection performance and the accuracy of the detected regions are evaluated. Table 1 shows the performance of candidate generation based on four different methods:

1) The proposed Bayesian method (Equation 2), where a combination of intensity, location and K2 shape feature (Equation 8) is used.
2) A Bayesian method, where instead of using the K2 shape feature, shape index is applied as shape model (Equation 9).
3) A non-Bayesian method, where only K2 probability (Equation 8) is calculated within the distance mask, and hysteresis thresholding is then directly applied on the K2 probability map for the initial candidate generation.
4) A 2D critical point (CP) based method (Slabaugh *et al*., 2010).

It can be seen that, of all the methods, the proposed Bayesian method provides superior performance regarding the detection sensitivity and false positives. Compared to both Bayesian methods with K2 shape

feature and that with shape index feature, the same detection sensitivity can be obtained. However, the Bayesian method with the K2 shape feature has 10 times fewer false positive regions than that of the shape index. The advantage of the K2 flow is that it is a "multi-scale" feature that is capable of detecting potential lesions of a wide range of sizes. Moreover, the Bayesian method has improved specificity (nearly half the detection regions) compared to the non-Bayesian with K2 only approach.

The proposed method may also provide an alternative approach for polyp segmentation. This is because the potential polyp candidates are calculated from the joint statistics of multi-features in the posterior probability (Equation 1 and 2) and this provides rich information for the proper lesion segmentation. The visual inspection of two polyp detection shown in Fig. 4f demonstrates the potential of the Bayesian method for both of candidate generation and segmentation. To further investigate the performance of the detected polyp regions, Dice's coefficient (R) is calculated between each detected polyp region and the ground truth. Each polyp boundary was manually delineated by a qualified radiologist. Fig. 5 shows the volume overlap ratios based on the Bayesian methods with two different shape models for all 83 detected polyp regions (excluding 10 polyps missed from both methods as indicated in Table 1). It can be seen that the proposed Bayesian method with the K2 shape feature gives a much better mean overlap ratio, with the mean overlap ratio increasing by 60%, compared to that using the SI feature.

Fig.4 Example of two polyps detection (a) CT sub-image; (b) Intensity probability; (c) Shape index probability; (d) Joint (Bayesian) probability based on intensity and SI probability; (e) K2 flow difference image; (f) Joint (Bayesian) probability based on intensity and K2 probability.

Table *1* *Comparison of initial candidates generation based on four different methods*

Methods	Bayesian with K2 shape feature and Intensity	Non-Bayesian with K2 shape feature only	Bayesian with SI and Intensity	2D CP based method
Sensitivity	95%	95%	95%	98%
FP/scan	124	228	1421	2310

Fig.5 Volume overlap ratio based on the two different shape models.

3.2 Candidate filtering

The Bayesian method can also be used as a filtering step to further remove false positive regions from initial polyp candidates. Those initial candidates are obtained from other shape based methods. The main procedure of the Bayesian method for candidate filtering is the same as that for initial candidate generation mentioned in Section 3.1. However, instead of using the distance probability (Equation 14) as a mask for calculating the conditional probability map of the joint intensity and shape likelihood for a candidate generation, in filtering, the conditional probability map is calculated within each potential polyp region.

In our previous work, we developed an automatic CT colonic polyp detection algorithm (Slabaugh *et al*., 2010). The aim of this experiment is to use the proposed Bayesian method to further remove false

regions. For each potential region, a polyp probability map based on the joint intensity and shape likelihood (Equation 2) is calculated. The intensity model is based on Equation 11, which the mean intensity is adaptively determined based on the candidate region size as defined in Equation 12; while the K2 shape feature is used for the shape model. A hysteresis thresholding and 3D labeling are then applied on each probability map. If a candidate region contains a set of 3D connected voxels with high probabilities of "polypness", the region is kept as a potential polyp region. Otherwise, the region is considered to be a non-polyp region and removed from the polyp candidates.

For a quantitative evaluation of the performance, the method has been tested on another independent dataset of 59 patients (118 CT volumes) of prone and supine volumes collected from four institutions, with total 75 polyps. Fig. 6 shows FROC curves based on our previous CAD algorithm and the further FP reduction based on the proposed Bayesian method. It can be seen that, with the same sensitivity, the Bayesian method reduces the FPs by an average of 24%. For example, with a sensitivity of 93.3%, the FP rate can be decreased from 6.2 per-volume to 4.7 per-volume after applying the Bayesian method. As we keep the same sensitivity for the proposed method, the improved curve looks shifted compared to the previous curve. This demonstrates the effectiveness of the proposed algorithm on the false positive reduction. (It is noted that, in this experiment, the sensitivity is measured per polyp that is, if a polyp is detected on either or both volumes, it is considered a true positive and false positives are measured per volume, as is the convention in CTC).

For comparison, Fig. 7 shows a FROC curve using FP reduction based on our earlier work (Ye *et al*., 2010) on the same dataset, where a uniform prior is used in the Bayesian probability calculation. The FP reduction based on the uniform prior is about 16% with no impact on sensitivity. It is clear that the Markov Random Field introduced in this chapter better models the prior probability by considering local interactions between neighboring voxels. Our new result improves the overall performance by an average of 8% compared to the uniform prior of our previous work.

Fig.6 Comparison ROC based on our previous CAD algorithm only and further FP reduction based on the proposed Bayesian method, where MRF is considered in the Bayesian probability calculation.

*Fig.7 Comparison ROC based on our previous CAD algorithm only and further FP reduction based on our earlier work (*Ye *et al*., 2010*), where a uniform prior is used in the Bayesian probability calculation.*

FUTURE RESEARCH DIRECTIONS

CAD methods for CTC have achieved significant progress during the last several years. To date, CAD has showed potential for detecting clinically significant polyps with high sensitivity and a relatively low number of FPs. However, CAD must be improved further to provide more accurate and reliable detection of polyps. To address this, in this chapter, we have introduced a novel detection method for colonic polyps in CT data. A Bayesian model maps the problem of polyp detection into a probability calculation, which is ideally suited to address the detection problem with the large uncertainty inherent to the medical imaging. Although three main features are considered for the joint probability calculation, the Bayesian framework is general and can be flexibly extended to incorporate other features. Indeed, one could

imagine incorporating patient informatics, such as patient age, family history of colorectal disease, or prior medical examinations etc., for robust detection. Patient informatics can be encoded either explicitly into prior probability or implicitly through the learning of likelihood parameter distributions from training data. By considering these informatics into Bayesian statistical framework, we are expecting to improve the robustness of the detection further.

Currently, laxative bowel preparation has been identified as one of the most important reasons for patients choose not to be screened (Beebe 2007). However, reduced or laxative-free bowel preparations introduce additional challenges to colon CAD, because they tend to introduce large amounts of solid fecal residue which mimics colonic polyps in shape. Some of the residue maybe tagged well, whereas others may not be tagged at all. CAD schemes may need to become more robust for such conditions to avoid large amount of false positive regions due to the fecal residue while maintaining clinically acceptable detection accuracy. To remove fecal-related FPs, one can try to register patient's colon between supine and prone volumes (Roth, *et al*., 2010). Precise registration of the two CT volumes of the patient colon could improve the specificity of polyp detection based upon a mobility analysis and greatly removing "moving objects" such as stool from initial candidates. However, robust automated registration of colon volumes itself remains a challenging task because of the substantial deformations of the colon. Alternatively, using our current framework, we can develop fecal-related image features and combine them into Bayesian statistics for the fecal specific FP reduction. One example of features would be texture features such as grey level co-occurrence (GLCM), wavelet coefficients, etc. However, although fecal tagging has been demonstrated to greatly improve distinguishing between stool and polyps, the tagging material itself might produce undesirable effects in CT values, which will distort results obtained by textural analysis.

Due to the natural flexibility of the Bayesian framework, other FP specific features (such as lipomas, etc.) can also be investigated and incorporated into the framework to improve the CAD performance in general.

CONCLUSION

We have presented an automatic detection method for colonic polyps in CT data. It calculates the probability of a polyp for each voxel through a unified Bayesian statistical model. The polyp likelihood is modeled using a combination of shape, intensity and location features. The second principal curvature flow is used as a shape model; while PVE is considered into modeling the polyp intensity distribution. The proposed method has been evaluated on a clinical dataset, both for candidate generation as well as filtering. Both qualitative and quantitative evaluation, based on CAD detection performance as well as volume overlap ratio demonstrate the potential of the proposed method. The method provides robust and consistent performance. In particular, the approach is capable of detecting and segmenting different types of polyps, such as the polyp attached to the colonic fold in Fig.4.

REFERENCES

Beebe, T.J., Johnson, C.D., Stoner, S.M., Anderson, K.J., & Limburg, P.J. (2007). Assessing attitudes toward laxative preparation in colorectal cancer screening and effects on future testing: potential receptivity to computed tomographic colonography. *Mayo Clinic Proceedings*, 82, 666-671.

Bogoni, L., Cathier, P., Dundar, M., Jerebko, A., Lakare, S., Liang, J., Periaswamy, S., Baker, M., & Macari, M. (2005). Computer-aided detection (CAD) for CT colonography: a tool to address a growing need. *British Journal of Radiology*, 78, S57–S62.

Gonzalez, R.C., & Woods, R.E. (2002). *Digital Image Processing*, Addison Wesley.

Jerebko, A., Lakare, S., Cathier, P., Periaswamy, S., & Bogoni, L. (2006). Symmetric Curvature Patterns for Colonic Polyp Detection. In Medical Image Computing and Computer-Assisted Intervention (*MICCAI)*, 4191, 169-176.

Johnson, C.D., Chen, M., Toledano, A., Heiken, J., Dachman, A.H.; Kuo, M.D., Menias, C., Stewert, B., Cheema, J.I., Obregon, R.G., Fidler, J.L., Zimmerman, P., Horton, K.M., Coakley, K., Iyer, R.B., Hara, A.K., Halvorsen, R.A., Casola, G., Yee, J., Herman, B.A., Burgart, L.J., & Limburg, P.J. (2008).

Accuracy of CT colonography for detection of large adenomas and cancers. *New England Journal of Medicine*, 259, 1207 – 1217.

Kim, D., Pickhardt, P., Taylor, A., Leung, W., Winter, T., Hinshaw, J.L., Gopal, D.V., Reichelderfer, M., Hsu, R.H., & Pfau, P.R. (2007). CT Colonography versus colonoscopy for the detection of advanced neoplasia. *New England Journal of Medicine*, 357, 1403-1412.

Kim, S.H., Lee, J.M., Lee, J.G., Kim, J.H., Lefere, P.A., Han, J.K., & Choi, B.I. (2007). Computer-aided detection of colonic polyps at CT colonography using a hessian matric-based algorithm: preliminary study. *Gastrointestinal Imaging*, 189, 41-51.

Koenderink, K., & Doorn, A.V. (1992). Surface shape and curvature scales. *Image and Vision Computing*, 10, 557-565.

Lawrence, E.M., Pickhardt, P.J., Kim, D.H., & Robbins, J.B. (2010). Colorectal polyps: stand-alone performance of computer-aided detection in a large asymptomatic screening population. In *Radiology*, 256, 791-798.

Li, S.Z. (1995). *Markov Random Field Modeling in Computer Vision*. Springer-Verlag.

Mendonca, P.R..S., Bhotika, R., Zhao, F., & Miller, J.V. (2007). Lung nodule detection via bayesian voxel labeling. In N.Karssemeijer & B.Lelieveldt (Eds), *IPMI*, 134-146.

Mendonca, P.R.S., Bhotika, R., Zhao, F., Melonakos, J., & Sirohey, S. (2008). Detection of polyps via shape and appearance modeling. *Proc. MICCAI 2008 Workshop: Computational and Visualization Challenges in the New Era of Virtual Colonoscopy*, 33-39.

Monga, O.,& Benayoun, S. (1995). Using partial derivatives of 3D images to extract typical surface features. *Computer Vision and Image Understanding*, 61, 171-189.

Paik, D.S., Beaulieu, C.F., Rubin, G.D., Acar, B., Jeffrey, R.B., Yee, J., Dey, J., & Napel, S. (2004). Surface normal overlap: a computer-aided detection algorithm with application to colonic polyps and lung nodules in helical CT. *IEEE Transactions on Medical Imaging*, 23(6), 661-675.

Pickhardt, P., Choi, J., & Hwang, I. (2003). Computed tomographic virtual colonoscopy to screen for colorectal neoplasia in asymptomatic adults. *New England Journal of Medicine*, 349(23), 2191-2200.

Raykar, V., Krishnapuram, B., Bi, J., Dundar, M., & Rao, R.B. (2008). Bayesian multiple instance learning: automatic feature selection and inductive transfer. In *International conference on machine learning (ICML)*.

Roth, H., McClelland, J., Modat, M., Boone, D., Hu, M., Ourselin, S., Slabaugh, G., Halligan, S., & Hawkes,D. (2010). Establishing spatial correspondence between the inner colon surfaces from prone and supine CT colonography. In *International Conference on Medical Image Computing and Computer Assisted Intervention (MICCAI), 497-504*, doi: 10.1007/978-3-642-15711-0_62.

Slabaugh, G., Yang, X., Ye, X., Boyes, R., & Beddoe, G. (2010). A Robust and Fast System for CTC Computer-Aided Detection of Colorectal Lesions. *Algorithms*, 3(1), 21-43.

Summers, R.M., Yao, J., Pickhardt, P., Franaszek, M., Bitter, I., Brickman, D., & Choi, J.R. (2005). Computed tomographic virtual colonoscopy computer-aided polyp detection in a screening population, *Gastroenterology*, 129, 1832-1844.

Sundaram, P., Zomorodian, A., Beaulieu, C., & Napel, S. (2008). Colon Polyp Detection using Smoothed Shape Operators: Preliminary Results. *Medical Image Analysis*, 12, 99–119.

Thirion, J. & Gourdon, A. (1992). Computing the differential characteristics of isointensity surface. *Computer Vision and Image Understanding*, 61, 190–202.

Vining, D.J., Ge, Y., Ahn, D.K., & Stelts, D.R. (1999). Virtual colonscopy with computer-assisted polyp detection. In Doi, K., MacMahon, H., Giger, M., & Hoffman, K.R. (Eds.), *Computer-Aided Diagnosis in Medical Imaging*, 445-452. Elsevier Science.

van Ravesteijn, V.F., van Wijk, C., Vos, F.M., Truyen, R., Peters, J., Stoker, J., & van Vliet, L. (2010). Computer Aided Detection of Polyps in CT Colonography using Logistic Regression. *IEEE Transactions on Medical Imaging*, 29(1), 120-131.

van Wijk, C., van Ravesteijn, V.F., Vos, F.M. & van Vliet, L.J. (2010). Detection and segmentation of colonic polyps on implicit isosurfaces by second principal curvature flow. *IEEE Transactions on Medical Imaging*, 29 (3), 688-698.

Webb, A. (1999). *Statistical Pattern Recognition*. Oxford University Press Inc., New York.

Winawer, S., Fletcher, R., Rex, D., Bond, J., Burt, R., Ferrucci, J., Ganiats, T., Woolf, S., Johnson, D., Kirk, L., Litin, S., & Simmang, C. (2003). Colorectal cancer screening and surveillance: Clinical guidelines and rationale—update based on new evidence. *Gastroenterology*, 124(2), 544-560.

Ye, X., Beddoe, G. & Slabaugh, G. (2010). A bayesian approach for false positive reduction in CTC CAD. *Proceedings of the MICCAI 2010 Workshop on Computational Challenges and Clinical Opportunities in Virtual Colonoscopy and Abdominal Imaging*, 49-54.

Yoshida, H. & Nappi, J. (2001). Three-dimensional computer-aided diagnosis scheme for detection of colonic polyps. *IEEE Transactions on Medical Imaging*, 20(12), 1261–1274.

Yoshida, H., Nappi, J., MacEneaney, P., Rubin, D.T., & Dachman, A.H. (2002). Computer-aided diagnosis scheme for detection of polypsat CT colonography. *Radiographics*, 22, 963-979.

Zrimec, T. & Wong, J.S. (2007). Improving computer aided disease detection using knowledge of disease appearance. In K.Kuhn (Eds.), *MedInfo*, IOS Press.

ADDITIONAL READING SECTION

Bhotika, R., Mendonca, P., Sirohey, S., Turner, W., Lee, Y., McCoy, J., Brown, R., & Miller, J. (2006). Part-based local shape models for colon polyp detection. *Medical image computing and computer-assisted intervention (MICCAI), 479-486.*

Dundar, M., & Bi, J. (2007). Joint optimization of cascaded classifiers for computer aided detection. *Computer Vision and Pattern Recognition (CVPR), 1-8.*

Faugeras, O. (1993). *Three-dimensional computer vision: A geometric view-point. Cambridge*, MA: MIT press.

Franaszek, M., Summers, R.M., Pickhardt, J., & Choi, J.R. (2006). Hybrid segmentation of colon filled with air and opacified fluid for CT colonography. *IEEE Transaction on Medical Imaging*, 25(3), 358-368.

Hong, W., Qiu, F., & Kaufman, A. (2006). A pipeline for computer aided polyp detection. *IEEE Transaction on Visualization and computer graphics*, 12(5), 861-868.

Iordanescu, G & Summers, R.M. (2004). Reduction of false positives on the rectal tube in computer-aided detection for CT colonography. *Medical Physics*, 31(10), 2855–2862.

Li, J.; Huang, A., Yao, J., Liu, J., Uitert, R.L.V., Petrick, N., & Summers, R.M. (2009). Optimizing computer-aided colonic polyp detection for CT colonography by evolving the pareto front. *Medical Physics*, 36, 201–212.

Liu, J., Wang, S., Kabadi, S., & Summers, R.M. (2009). High Performance Computer Aided Detection System for Polyp Detection in CT Colonography with Fluid and Fecal Tagging. In *Proceedings of the SPIE*, 7260, 72601B. doi:10.1117/12.811654.

Nappi, J. & Yoshida, H. (2008). Automated scheme for preparation-independent detection of colorectal lesions with comparison to conventional CAD in CT colonography. *Proc. MICCAI 2008 Workshop: Computational and Visualization Challenges in the New Era of Virtual Colonoscopy*, 127-134.

Obuchowski, N.A. (2005). Fundamentals of Clinical Research for Radiologists: ROC Analysis. *American Journal of Roentgenology (AJR)*, 184: 364-372.

Pickhardt, P.J. (2004). Translucency rendering in 3D endoluminal CT colonography: a useful tool for increasing polyp specificity and decreasing interpretation time. *American Journal of Roentgenology (AJR)*, 183: 429-463.

Qiu, F., Marino, J., & Kaufman, A. (2008). Computer Aided Polyp Detection with Texture Analysis. In *MICCAI Workshop on Computational and Visualization Challenges in the New Era of Virtual Colonoscopy*.

Suzuki, K., Rockey, D.C., & Dachman, A.H. (2010). CT colonography: Computer-aided detection of false-negative polyps in a multicenter clinical trial. Medical Physics, 30, 2–21.

Suzuki, K., Yoshida, H., Nappi, J., & Dachman, A. (2006). Massive-training artificial neural network _MTANN_ for reduction of false positives in computer-aided detection polyps: Suppression of rectal tubes. *Medical Physics*, 33(10), 3814–3824.

Suzuki, K., Yoshida, H., Nappi, J., Armato, S.G., & Dachman, A.H. (2008). Mixture of expert 3D massive-training ANNs for reduction of multiple types of false positives in CAD for detection of polyps in CT colonography. *Medical Physics*, 35, 694–703.

Suzuki, K., Zhang, J., & Xu, J. (2010). Massive-training artificial neural network coupled with Laplacian –eigenfunction-based dimensionality reduction for computer-aided detection of polyps in CT colonography. *IEEE Transactions on Medical Imaging*, 29(11), 1907-1917.

Tu, Z., Zhou, X.S., Barbu, A., Bogoni, L., & Comaniciu, D. (2006). Probabilistic 3D polyp detection in CT images: the role of sample alignment. In *Computer Vision and Pattern Recognition (CVPR)*, vol.2, 1544-1551.

Wang, T., Lu, H., Zhang, J., Zhang, G., Liu, X., & Z, Z.L. (2008). Computer-aided detection for virtual colonoscopy based on 3D texture analysis. In *International Congress on Computer Assisted Radiology and Surgery (CARS)*.

Wang, S., Yao, J., & Summers, R.M. (2008). Improved classifier for computer-aided polyp detection in CT colonography by nonlinear dimensionality reduction. Medical Physics, 35(4), 1377–1386.

Yoshida, H. (Ed.) (2008). *Proceedings of the MICCAI 2008 workshop on computational and visualization challenges in the new era of virtual colonoscopy*. New York City, NY, USA.

Yoshida, H., and Cai, W. (Ed.) (2010). *Proceedings of the MICCAI 2010 workshop on computational challenges and clinical opportunities in virtual colonoscopy and abdominal imaging*, Beijing, China.

Yoshida, H. & Dachman, A.H. (2005). CAD techniques, challenges, and controversies in computed tomographic colonography. *Abdominal Imaging*, 30(1), 26–41.

Zhao, L., Botha, C.P., Bescos, J.O., Truyen, R., Vos, F.M., & Post, F.H. (2006). Lines of curvature for polyp detection in virtual colonoscopy. *IEEE Transaction on Visualization and computer graphics*, 12(5), 885-892.

Zheng, Y., Yang, X., & Beddoe, G. (2007). Reduction of false positives in polyp detection using weighted support vector machines. In *Proceeding of EMBC, 4433-4436*.

Zhu, H., Liang, Z., Pickhardt, P.J., Barish, M.A., Fan, Y., Lu, H., Posniak, E.J., Richards, R.J., & Cohen, H.L. (2010). Increasing computer-aided detection specificity by projection features for CT colonography. *Medical Physics*, 37(4), 1468-1481.

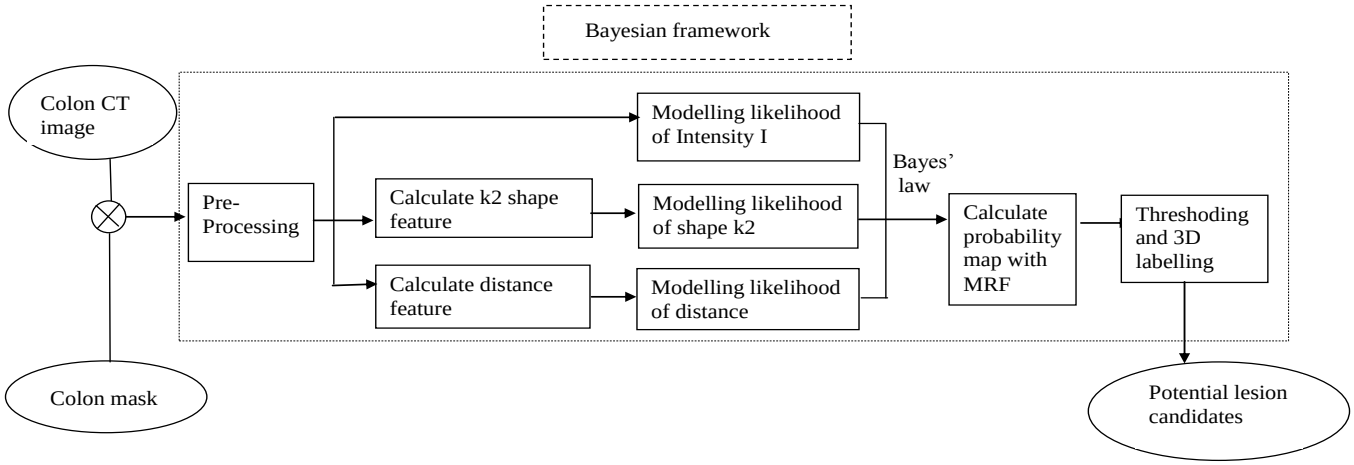

Fig.1 Block diagram of the proposed Bayesian method

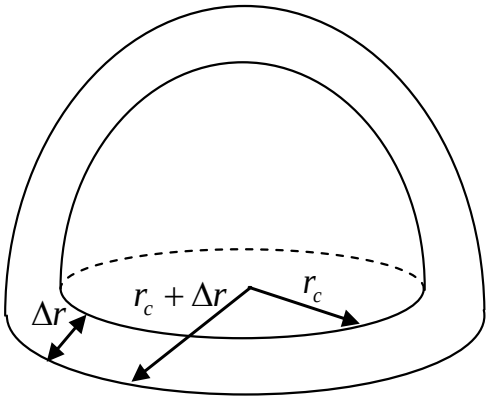

Fig.2 A schematic diagram of colonic polyp

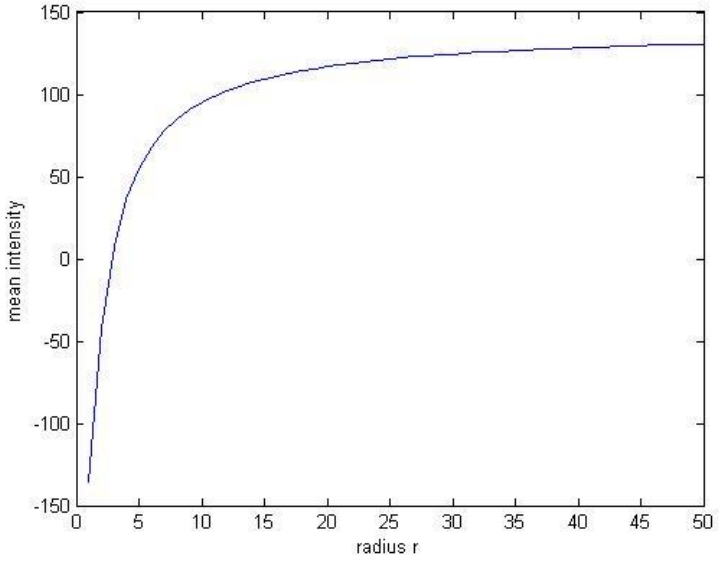

Fig.3 An example of mean intensity ($\mu_I(r)$) of the polyp varying with the radius size (r) based on Equation 12.

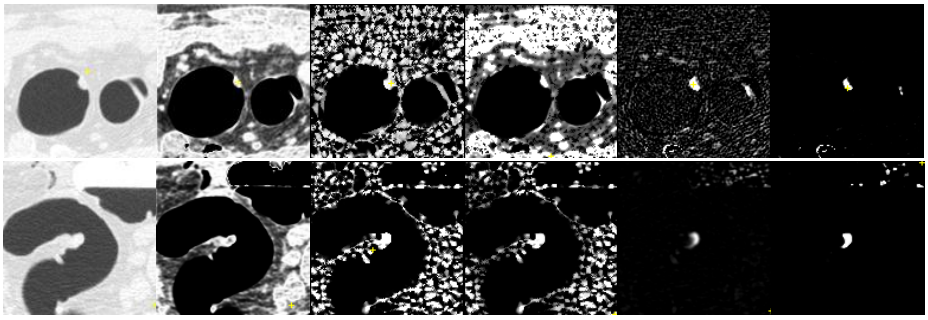

(a) (b) (c) (d) (e) (f)

Fig.4. Example detection of two polyps (a) CT sub-image; (b) Intensity probability; (c) Shape index probability; (d) Joint (Bayesian) probability based on intensity and SI probability; (e) K2 flow difference image; (f) Joint (Bayesian) probability based on intensity and K2 probability.

Table1 Comparison of initial candidate generation based on four different methods

Methods	Bayesian with K2 shape feature and Intensity	Non-Bayesian with K2 shape feature only	Bayesian with SI and Intensity	2D CP based method
Sensitivity	95%	95%	95%	98%
FP/scan	124	228	1421	2310

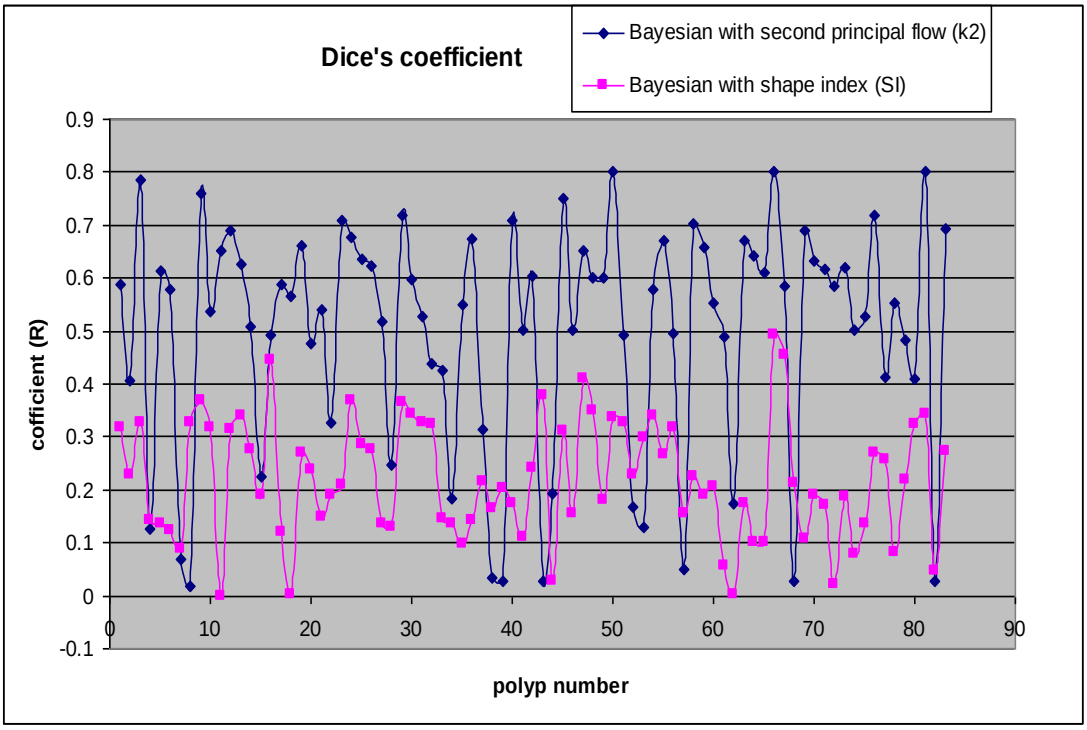

Fig.5 Volume overlap ratio based on the two different shape models

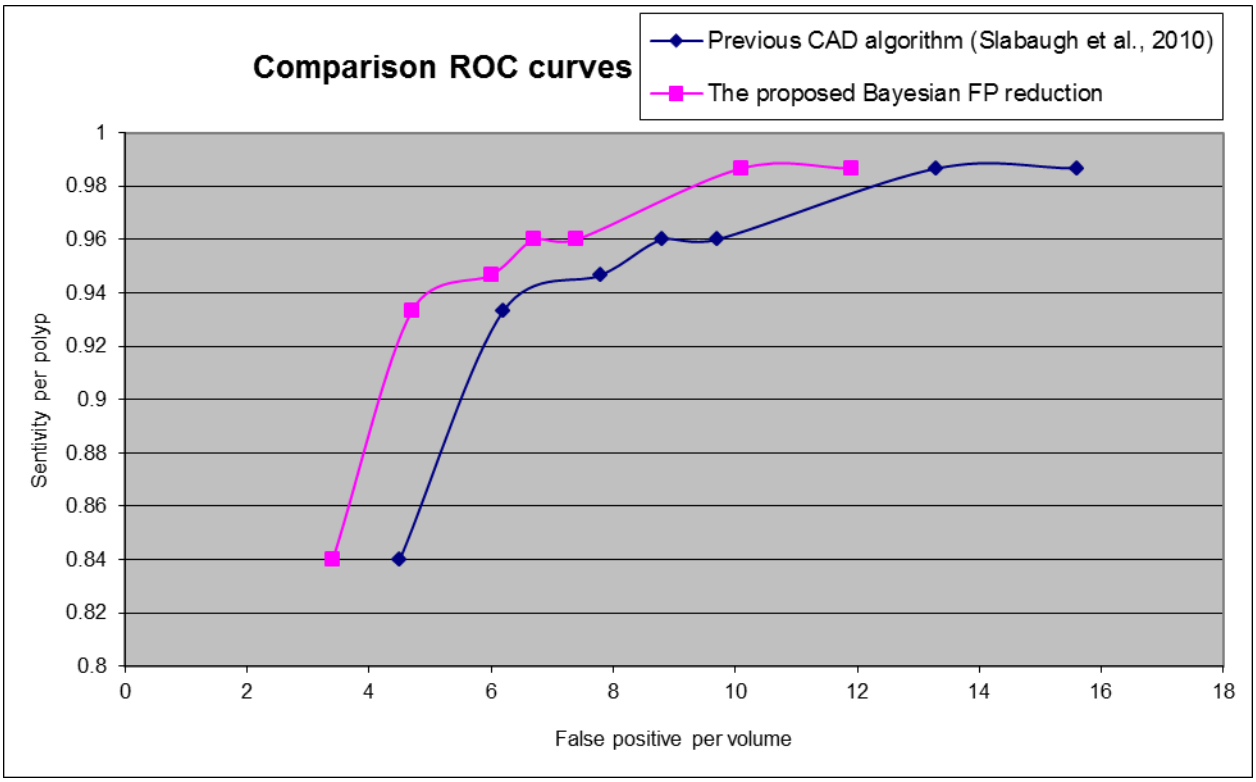

Fig.6 Comparison ROC based on our previous CAD algorithm only and further FP reduction based on the proposed Bayesian method, where MRF is considered in the Bayesian probability calculation.

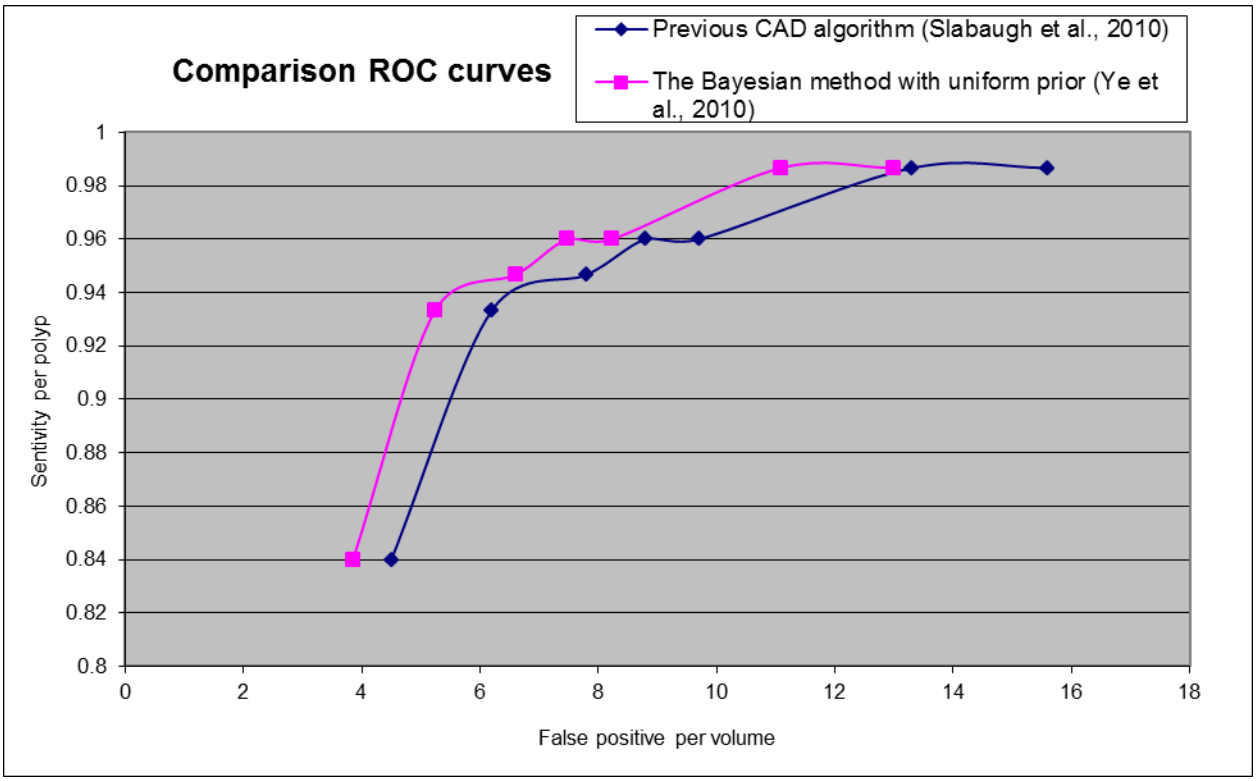

Fig.7 Comparison ROC based on our previous CAD algorithm only and FP reduction based on our earlier work (Ye *et al*., 2010), where a uniform prior is used in the Bayesian probability calculation.

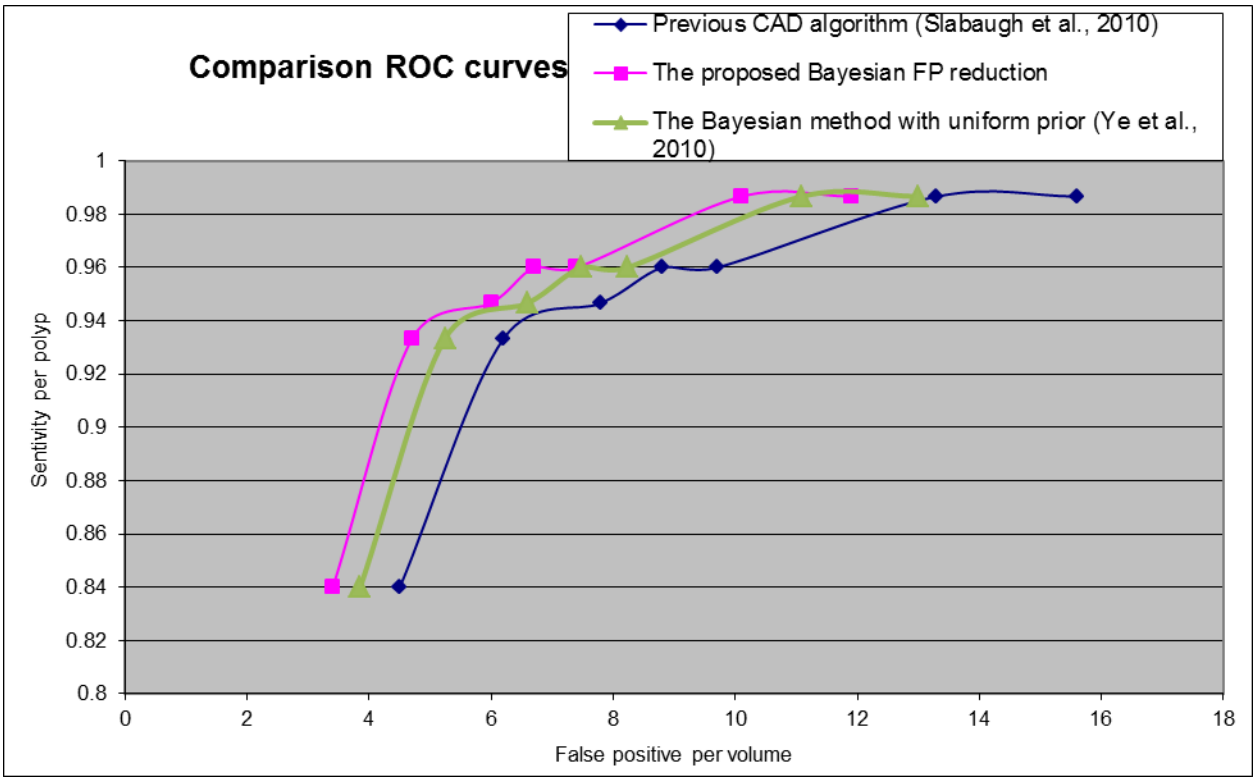
Comparison ROC curves
Previous CAD algorithm (Slabaugh et al., 2010)
The proposed Bayesian FP reduction
The Bayesian method with uniform prior (Ye et al., 2010)
Sentivity per polyp
1
0.98
0.96
0.94
0.92
0.9
0.88
0.86
0.84
0.82
0.8
0
2
4
6
8
10
12
14
16
18
False positive per volume